PCCP

Physical Chemistry Chemical Physics

This paper is published as part of a PCCP Themed Issue on:

New Frontiers in Surface-Enhanced Raman Scattering

Guest Editor: Pablo Etchegoin

Editorial

***Quo vadis* surface-enhanced Raman scattering?**
Phys. Chem. Chem. Phys., 2009
DOI: 10.1039/b913171j

Perspective

Surface-enhanced Raman spectroscopy of dyes: from single molecules to the artists' canvas
Kristin L. Wustholz, Christa L. Brosseau, Francesca Casadio and Richard P. Van Duyne, *Phys. Chem. Chem. Phys.*, 2009
DOI: 10.1039/b904733f

Communication

Tip-enhanced Raman scattering (TERS) of oxidised glutathione on an ultraflat gold nanoplate
Tanja Deckert-Gaudig, Elena Bailo and Volker Deckert, *Phys. Chem. Chem. Phys.*, 2009
DOI: 10.1039/b904735b

Papers

Self-assembly of α,ω-aliphatic diamines on Ag nanoparticles as an effective localized surface plasmon nanosensor based in interparticle hot spots
Luca Guerrini, Irene Izquierdo-Lorenzo, José V. Garcia-Ramos, Concepción Domingo and Santiago Sanchez-Cortes, *Phys. Chem. Chem. Phys.*, 2009
DOI: 10.1039/b904631c

Single-molecule vibrational pumping in SERS
C. M. Galloway, E. C. Le Ru and P. G. Etchegoin, *Phys. Chem. Chem. Phys.*, 2009
DOI: 10.1039/b904638k

Silver nanoparticles self assembly as SERS substrates with near single molecule detection limit
Meikun Fan and Alexandre G. Brolo, *Phys. Chem. Chem. Phys.*, 2009
DOI: 10.1039/b904744a

Gated electron transfer of cytochrome c_6 at biomimetic interfaces: a time-resolved SERR study
Anja Kranich, Hendrik Naumann, Fernando P. Molina-Heredia, H. Justin Moore, T. Randall Lee, Sophie Lecomte, Miguel A. de la Rosa, Peter Hildebrandt and Daniel H. Murgida, *Phys. Chem. Chem. Phys.*, 2009
DOI: 10.1039/b904434e

Investigation of particle shape and size effects in SERS using *T*-matrix calculations
Rufus Boyack and Eric C. Le Ru, *Phys. Chem. Chem. Phys.*, 2009
DOI: 10.1039/b905645a

Plasmon-dispersion corrections and constraints for surface selection rules of single molecule SERS spectra
S. Buchanan, E. C. Le Ru and P. G. Etchegoin, *Phys. Chem. Chem. Phys.*, 2009
DOI: 10.1039/b905846j

Redox molecule based SERS sensors
Nicolás G. Tognalli, Pablo Scodeller, Victoria Flexer, Rafael Szamocki, Alejandra Ricci, Mario Tagliazucchi, Ernesto J. Calvo and Alejandro Fainstein, *Phys. Chem. Chem. Phys.*, 2009
DOI: 10.1039/b905600a

Controlling the non-resonant chemical mechanism of SERS using a molecular photoswitch
Seth Michael Morton, Ebo Ewusi-Annan and Lasse Jensen, *Phys. Chem. Chem. Phys.*, 2009
DOI: 10.1039/b904745j

Interfacial redox processes of cytochrome b_{562}
P. Zuo, T. Albrecht, P. D. Barker, D. H. Murgida and P. Hildebrandt, *Phys. Chem. Chem. Phys.*, 2009
DOI: 10.1039/b904926f

Surface-enhanced Raman scattering of 5-fluorouracil adsorbed on silver nanostructures
Mariana Sardo, Cristina Ruano, José Luis Castro, Isabel López-Tocón, Juan Soto, Paulo Ribeiro-Claro and Juan Carlos Otero, *Phys. Chem. Chem. Phys.*, 2009
DOI: 10.1039/b903823j

SERS imaging of HER2-overexpressed MCF7 cells using antibody-conjugated gold nanorods
Hyejin Park, Sangyeop Lee, Lingxin Chen, Eun Kyu Lee, Soon Young Shin, Young Han Lee, Sang Wook Son, Chil Hwan Oh, Joon Myong Song, Seong Ho Kang and Jaebum Choo, *Phys. Chem. Chem. Phys.*, 2009
DOI: 10.1039/b904592a

Nanospheres of silver nanoparticles: agglomeration, surface morphology control and application as SERS substrates
Xiao Shuang Shen, Guan Zhong Wang, Xun Hong and Wei Zhu, *Phys. Chem. Chem. Phys.*, 2009
DOI: 10.1039/b904712c

SERS enhancement by aggregated Au colloids: effect of particle size
Steven E. J. Bell and Maighread R. McCourt, *Phys. Chem. Chem. Phys.*, 2009
DOI: 10.1039/b906049a

Towards a metrological determination of the performance of SERS media
R. C. Maher, T. Zhang, L. F. Cohen, J. C. Gallop, F. M. Liu and M. Green, *Phys. Chem. Chem. Phys.*, 2009
DOI: 10.1039/b904621f

Ag-modified Au nanocavity SERS substrates
Emiliano Cortés, Nicolás G. Tognalli, Alejandro Fainstein, María E. Vela and Roberto C. Salvarezza, *Phys. Chem. Chem. Phys.*, 2009
DOI: 10.1039/b904685m

Surface-enhanced Raman scattering studies of rhodanines: evidence for substrate surface-induced dimerization
Saima Jabeen, Trevor J. Dines, Robert Withnall, Stephen A. Leharne and Babur Z. Chowdhry, *Phys. Chem. Chem. Phys.*, 2009
DOI: 10.1039/b905008f

Characteristics of surface-enhanced Raman scattering and surface-enhanced fluorescence using a single and a double layer gold nanostructure
Mohammad Kamal Hossain, Genin Gary Huang, Tadaaki Kaneko and Yukihiro Ozaki, *Phys. Chem. Chem. Phys.*, 2009
DOI: 10.1039/b903819c

High performance gold nanorods and silver nanocubes in surface-enhanced Raman spectroscopy of pesticides
Jean Claudio Santos Costa, Rômulo Augusto Ando, Antonio Carlos Sant'Ana, Liane Marcia Rossi, Paulo Sérgio Santos, Márcia Laudelina Arruda Temperini and Paola Corio, *Phys. Chem. Chem. Phys.*, 2009
DOI: 10.1039/b904734d

Water soluble SERS labels comprising a SAM with dual spacers for controlled bioconjugation
C. Jehn, B. Küstner, P. Adam, A. Marx, P. Ströbel, C. Schmuck and S. Schlücker, *Phys. Chem. Chem. Phys.*, 2009
DOI: 10.1039/b905092b

Chromic materials for responsive surface-enhanced resonance Raman scattering systems: a nanometric pH sensor
Rômulo A. Ando, Nicholas P. W. Pieczonka, Paulo S. Santos and Ricardo F. Aroca, *Phys. Chem. Chem. Phys.*, 2009
DOI: 10.1039/b904747f

Gated electron transfer of cytochrome c_6 at biomimetic interfaces: a time-resolved SERR study†

Anja Kranich,[a] Hendrik Naumann,[a] Fernando P. Molina-Heredia,[b] H. Justin Moore,[c] T. Randall Lee,[c] Sophie Lecomte,[d] Miguel A. de la Rosa,[b] Peter Hildebrandt*[a] and Daniel H. Murgida*[e]

Received 4th March 2009, Accepted 30th April 2009
First published as an Advance Article on the web 1st June 2009
DOI: 10.1039/b904434e

The electron shuttle heme protein Cyt-c_6 from the photosynthetic cyanobacterium *Nostoc* sp. PCC 7119 was immobilized on nanostructured Ag electrodes coated with SAMs that mimic different possible interactions with its natural reaction partner PSI. The structure, redox potential, and electron-transfer dynamics of the SAM–Cyt-c_6 complexes were investigated by TR-SERR spectroelectrochemistry. It is shown that the heterogeneous electron-transfer process is gated both in electrostatic and hydrophobic–hydrophilic complexes. At long tunneling distances, the reaction rate is controlled by the tunneling probability, while at shorter distances or higher driving forces, protein dynamics becomes the rate-limiting event.

Introduction

Cytochrome c_6 (Cyt-c_6) is a monomeric soluble heme protein found in photosynthetic organisms, such as some cyanobacteria and green algae. Its natural function is transporting electrons up taken from the b_6f membrane-bound complex to photosystem I (PSI).[1] In plants, this role is exclusively played by the copper protein plastocyanin (Pc), but several lower organisms have the ability to produce either Pc or Cyt-c_6 depending on the bioavailability of Cu and Fe.[2] This is the case of the cyanobacterium *Nostoc* (formerly *Anabaena*) PCC 7119 (hereinafter *Nostoc*).

Cyt-c_6 from *Nostoc* is a basic protein (pI $\approx$ 9) with a molecular mass of 9.7 kDa.[3] Although its three-dimensional structure has not been resolved, sequence homology and spectroscopic evidence indicate that the heme iron is coordinated by histidine 19 and methionine 58 as axial ligands, yielding a six-coordinated low spin (6c-LS) heme within the pH range 5–11.[3]

Transient absorption spectroscopy shows that *in vitro* interprotein electron transfer (ET) from *Nostoc* Cyt-c_6 to PSI follows biphasic kinetics. These results were interpreted in terms of a gated ET mechanism.[4–6] Structural modeling of Cyt-c_6, as well as kinetic experiments with point mutants, suggests the existence of two areas on the protein surface responsible for the interactions with PSI. A basic patch defined by residues Lys62, Lys66, and possibly Arg64 is believed to provide the long-range electrostatic interactions that drive the formation of the initial interprotein complex. It is hypothesized that docking through this site fails to provide an efficient electron pathway and, thus, transient rearrangement of the complex is required for efficient electron transfer to take place. The hydrophobic patch located in close vicinity to the partially exposed heme edge is considered essential for establishing the optimal electron pathway (Fig. 1).[4,7,8]

On the other hand, NMR investigations of the transient complex between Cyt-c_6 and the Cyt-f soluble truncated subunit of the b_6f complex from *Nostoc* indicate that the interprotein contact region is mainly comprised of non-polar

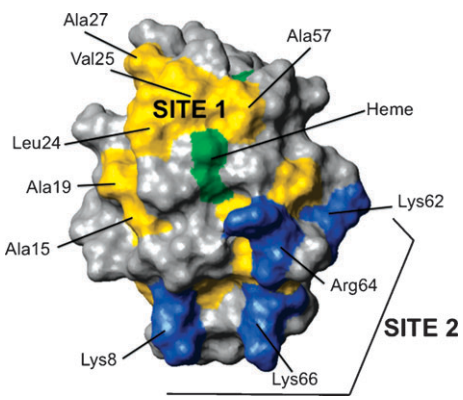

Fig. 1 Functional areas of *Nostoc* cytochrome Cyt-c_6. Non-polar residues at site 1 are marked in yellow, positively charged residues at site 2 are in blue, and the heme group is in green. The surface map corresponds to the lowest energy conformer inferred from the NMR protein structure.[9,10]

[a] *Institut für Chemie, Technische Universität Berlin. Str. des 17. Juni 135, Sekr. PC, 14, D10623-Berlin, Germany. E-mail: hildebrandt@chem.tu-berlin.de*
[b] *Instituto de Bioquímica Vegetal y Fotosíntesis, Centro de Investigaciones Científicas Isla de la Cartuja, Universidad de Sevilla y Consejo Superior de Investigaciones Científicas, Sevilla, Spain*
[c] *Department of Chemistry, University of Houston, Houston, TX 77204-5003, USA*
[d] *CBMN, CNRS-Université Bordeaux 1 (UMR5248), 2 rue Robert d'Escarpit, F-33607 Pessac, France*
[e] *Departamento de Química Inorgánica, Analítica y Química Física/ INQUIMAE-CONICET, Facultad de Ciencias Exactas y Naturales, Universidad de Buenos Aires. Ciudad Universitaria, Pab. 2, piso 1, C1428EHA-Buenos Aires, Argentina. E-mail: dhmurgida@qi.fcen.uba.ar*

† Electronic supplementary information (ESI) available: RR spectral parameters and kinetic simulations. See DOI: 10.1039/b904434e

residues (*ca.* 61%).[9] Similar studies on Cyt-c_6–PSI complexes reveal that both basic and non-polar amino acids are involved in the interactions.[10] More recently, CW-EPR and ENDOR experiments demonstrated the coexistence of two LS ferric forms, one of them highly anisotropic. The finding was related to the need for structural flexibility of Cyt-c_6 in its interactions with the two different redox partners.[11,12]

In this work, we present a study of the interactions of *Nostoc* Cyt-c_6 with biomimetic surfaces having different electrostatic and hydrophobic properties, and the impact of these interactions on the dynamics of the ET reaction. Besides the wild type (WT) protein, we have studied the mutant M58H, in which the sixth axial ligand methionine has been replaced by a histidine to obtain a bis-histidine coordination.

The model systems consist of nanostructured Ag electrodes coated by self-assembled monolayers (SAMs) of alkanethiols having varying chain lengths and terminal functionalities.[13] Adsorption and ET dynamics are monitored by stationary and time-resolved (TR) surface-enhanced resonance Raman (SERR) spectroelectrochemistry.[14]

Experimental

Chemicals

16-Mercaptohexadecanoic acid (C_{15}-COOH), 11-mercapto-undecanoic acid (C_{11}-COOH), 11-mercapto-1-undecanol (C_{11}-OH), 1-mercaptododecane (C_{11}-CH_3), sucrose, potassium chloride, potassium sulfate, and potassium phosphate were purchased from Sigma-Aldrich and used without further purification. 16-Mercaptohexadecanol (C_{16}-OH) was synthesized as described previously.[15,16] 1-Mercaptoheptadecane (C_{16}-CH_3) was prepared from the corresponding bromide by nucleophilic displacement with thioacetate followed by basic deprotection and standard purification methods.

Water used in all experiments was purified by a Millipore system and its resistance was more than 18 MΩ.

Protein expression and purification

Wild type cytochrome c_6 and its M58H mutant from *Nostoc* sp. PCC7119 were expressed under aerobic conditions in *Escherichia coli* MC1061-transformed cells and purified as described elsewhere.[8] The purity of the protein preparations was greater than 95% as judged from the ratio of absorbance at 553 and 280 nm for reduced Cyt-c_6 and from the absence of other visible bands on Coomassie-stained SDS-PAGE. Protein concentrations were determined using an extinction coefficient ε_{553} = 26.2 mM^{-1} cm^{-1} for reduced Cyt-c_6.[3]

Redox titrations

The redox potential value in solution for the M58H mutant was determined by UV-Vis potentiometric titrations as previously described,[3,17] by following absorbance changes at 554 minus 570 nm. Errors of the experimental determinations were less than 10 mV.

Resonance Raman

Protein samples were placed inside a cylindrical quartz cell that is rotated at *ca.* 5 Hz to avoid laser-induced degradation. Spectra were measured at room temperature in back-scattering geometry using a confocal microscope coupled to a single stage spectrograph (Jobin Yvon, LabRam 800 HR) equipped with a 2400 lines per mm grating and a liquid-nitrogen-cooled back-illuminated CCD detector. Elastic scattering was rejected by a Notch filter. All spectra reported here were measured with the 413 nm line of a cw krypton ion laser (Coherent Innova 300 c) focused on the sample by means of a long working distance objective (20×; N.A. 0.35). Typically, experiments were performed with laser powers of *ca.* 5 mW at the sample. Effective acquisition times were *ca.* 10–20 s with an increment per data point of 0.57 cm^{-1}.

Electrode modification

Silver-ring electrodes were mechanically polished with 3 M polishing films from 30 to 1 micron grade. After washing, electrodes were subjected to oxidation–reduction cycles in 0.1 M KCl to create a SER-active nanostructured surface. Subsequently, the electrodes were incubated in 1 mM ethanolic solutions of the alkanethiols for 24 h, rinsed, and transferred to the spectroelectrochemical cell.

Surface-enhanced resonance Raman

The spectroelectrochemical cell for SERR measurements has been described elsewhere.[18] Briefly, a Pt wire and a Ag/AgCl electrode are used as counter and reference electrodes, respectively. All potentials cited in this work refer to the Ag/AgCl (3 M KCl) electrode. The working electrode is an 8 mm diameter and 2.5 mm height silver ring mounted on a shaft that is rotated at *ca.* 5 Hz to avoid laser-induced sample degradation. The electrolyte solution (12.5 mM phosphate buffer, pH = 7.0; 12.5 mM K_2SO_4) was bubbled prior to the measurements with catalytically purified oxygen-free argon, and Ar overpressure was maintained during the experiments. Protein was added to the electrochemical cell from a stock solution to form a 0.3 μM solution and incubated at room temperature for *ca.* 15 min before starting the experiments. SERR spectra were measured in back-scattering geometry as described in the previous section. Typically, experiments were performed with laser powers of 2.5–5 mW at the sample, effective acquisition times between 1 and 30 s, and increments per data point of 0.57 cm^{-1}. For TR SERR experiments, potential jumps of variable height and duration were applied to trigger the reaction. SERR spectra were measured at variable delay times after each jump. Synchronization of potential jumps and measuring laser pulses was achieved with a home-made four-channel pulse-delay generator. The measuring pulses were generated by passing the cw laser beam through two consecutive laser-intensity modulators (Linos), which give a total extinction better than 1 : 50 000 and a time response of *ca.* 20 ns.

After background subtraction, the spectra were treated by component analysis in which the spectra of the individual species were fitted to the measured spectra using home-made analysis software. All experiments were repeated several times to ensure reproducibility.

Kinetic simulations

Kinetic analysis was performed using GNU octave software. The set of differential equations that describe the kinetics for the proposed reaction mechanism was solved numerically, yielding concentration profiles for the four chemical species involved. Five adjustable parameters (A, β, λ, k_1, and k_2; *vide infra*) were varied until minimizing the standard deviations with respect to the experimental data. In this procedure, the experimental data set corresponds to a large number of experiments that include different chain lengths of the SAMs and various driving forces and solution viscosities. Further details are given in the following sections.

Results and discussion

Resonance Raman spectroscopy in solution

Wild type Cyt-c_6 and its M58H mutant were first characterized by RR spectroscopy in solution, *i.e.* under conditions that guarantee preservation of the native structures, as a prerequisite for the subsequent studies of the immobilized proteins.

Assuming an idealized D_{4h} symmetry for the porphyrin chromophore, resonance enhancement of heme proteins is only expected for the *gerade* in-plane vibrational modes. Specifically, under Soret-band excitation, RR spectra are dominated by the totally symmetric modes A_{1g}, which gain intensity *via* the A-term enhancement mechanism.[19] Due to the lower symmetry that characterizes actual hemes, also non-totally symmetric modes B_{1g}, A_{2g}, and B_{2g} gain intensity, but to a lesser extent.[20,21] RR spectra of ferrous and ferric WT-Cyt-c_6 in the so-called marker band region (*ca.* 1300–1700 cm^{-1})[22] are shown in Fig. 2.

Vibrational modes observed in this spectral region are largely derived from C–C and C–N stretching vibrations of the porphyrin. Due to the increased electron back donation of Fe^{2+} compared to Fe^{3+} into the π^* orbital of the porphyrin, which weakens the C–N bonds, most bands are significantly up-shifted upon oxidation. Moreover, they are also sensitive markers of the spin and ligation pattern of the heme iron.[13,14]

Band positions, shapes (Lorentzian), widths, and relative intensities observed in the RR spectra of ferrous and ferric WT-Cyt-c_6 are characteristic of 6c-LS type c hemes with the Met–His axial coordination pattern,[13,23,24] as predicted from the sequence and in analogy to equivalent proteins from other organisms.[3,4,25]

For the M58H mutant, RR spectra exhibit only slight shifts of most bands with respect to the WT protein. For example, in the reduced form, the most prominent band ν_4 appears at 1358 cm^{-1} for the mutant compared to 1360 cm^{-1} for the WT. These small spectral changes are compatible with the axial-ligand substitution of methionine by histidine as neither the spin state nor the coordination number of the heme iron are changed.[13,23,24] Complete sets of spectral parameters are given in ESI†.

RR intensities are proportional to the concentration of the species. Proportionality factors (F) for the reduced and oxidized proteins were determined from the intensity ratios reduced–oxidized of RR spectra measured under identical conditions, *i.e.*, adopting $F = 1$ for the ferric form. The value of 0.143 obtained for both ferrous forms (WT and M58H) is used in the subsequent sections for quantification of the redox equilibria and dynamics.

Protein adsorption and redox equilibria

It has been proposed that Cyt-c_6 employs two distinct sites for the interaction with its redox partner PSI: a positively charged domain responsible for efficient docking and a hydrophobic patch that provides an optimized but transient ET pathway (see Introduction). With these premises in mind, we have investigated the immobilization of Cyt-c_6 on nanostructured Ag electrodes coated with uncharged SAMs of variable hydrophobicity as well as negatively charged SAMs. Protein adsorption was monitored by SERR under Soret-band excitation, *i.e.* under conditions that ensure sensitive and selective detection solely of Cyt-c_6 adsorbed molecules. Fig. 3 shows normalized SERR intensities measured for Cyt-c_6 adsorbed on mixed SAMs composed of variable ratios of 1-mercaptododecane and 11-mercapto-1-undecanol (C_{11}-CH_3 and C_{11}-OH, respectively).

Optimal adsorption is achieved for compositions around 1 : 1, while no adsorption is observed for SAMs of the pure

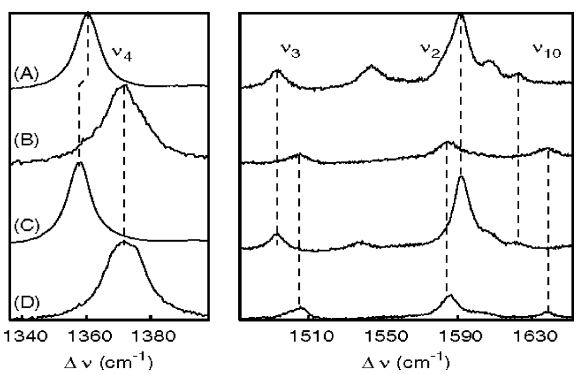

Fig. 2 RR spectra of: (A) ferrous WT-Cyt-c_6, (B) ferric WT-Cyt-c_6, (C) ferrous M58H-Cyt-c_6, and (D) ferric M58H-Cyt-c_6. All measurements were performed with 413 nm laser excitation. Bands are labeled according to Hu *et al.*[21]

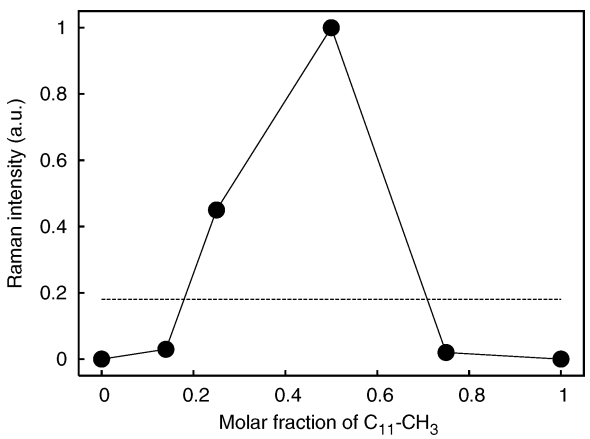

Fig. 3 Normalized SERR intensity of WT-Cyt-c_6 adsorbed on C_{11}-CH_3/C_{11}-OH mixed SAMs of variable composition (circles and solid line). The dashed line represents the normalized SERR intensity obtained for WT-Cyt-c_6 adsorbed on a C_{10}-COOH pure SAM.

alkanethiol components. Note that the compositions indicated in Fig. 3 correspond to the solution compositions utilized for self-assembly and not to the final surface compositions.[26]

For a negatively charged SAM of comparable length composed of 11-mercaptoundecanoic acid (C_{10}-COOH), the amount of adsorbed protein is about one-fifth of the maximum value obtained for C_{11}-CH_3/C_{11}-OH mixed SAMs. At pH 7.0, employed in all the studies reported here, the degree of ionization of the C_{10}-COOH SAMs is about 10%.[27] These results indicate that optimal adsorption of Cyt-c_6 requires an adequate balance of hydrophobic and hydrophilic interactions, while electrostatic forces lead to relatively weak adsorption.

This behavior is in contrast to horse heart and yeast cytochromes *c*, which have significantly larger dipole moments and better defined positive patches around the partially exposed heme,[13,14,28–30] but resemble that of cytochrome c_{552} which exhibits a hydrophobic binding domain surrounding the heme pocket.[15,16]

For both modes of immobilization, the native structure of Cyt-c_6 is retained, at least at the level of the active site. This is inferred from the SERR spectra of the adsorbed protein, which are essentially identical to the corresponding RR spectra of the native protein in solution (Fig. 4).

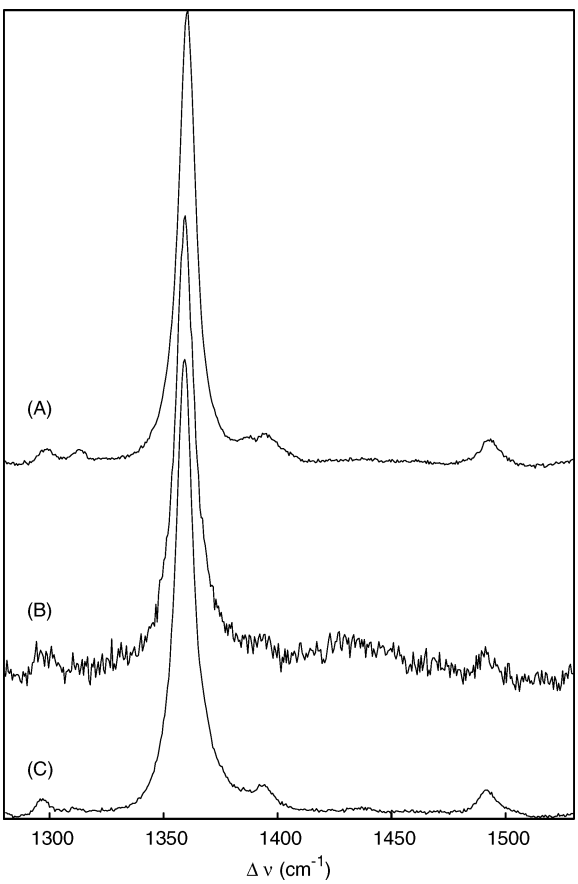

Fig. 4 Comparison of the RR spectrum of dithionite-reduced WT-Cyt-c_6 in solution (A) and SERR spectra of the electrochemically reduced protein adsorbed on C_{15}-COOH (B) and on C_{16}-CH_3/C_{16}-OH (C) SAMs in the spectral region of the ν_3 and ν_4 modes.

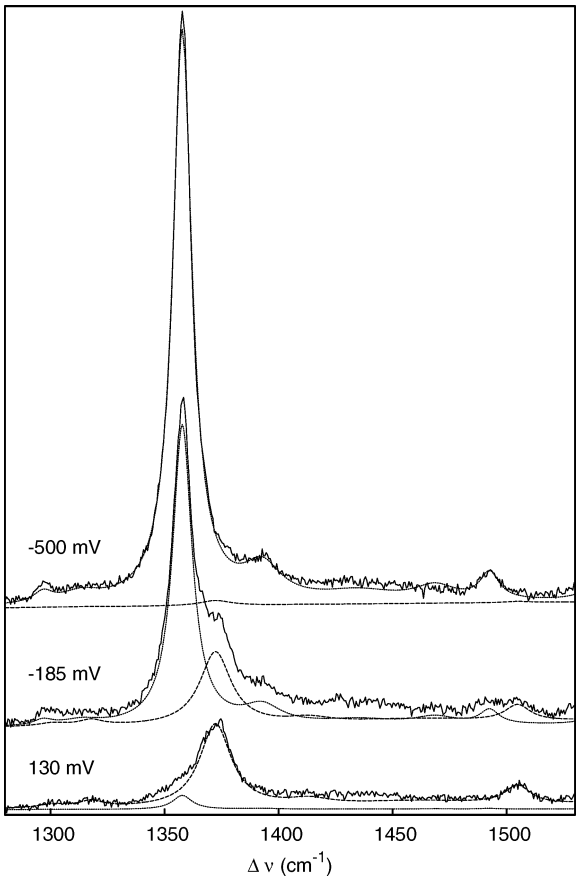

Fig. 5 SERR spectra of M58H-Cyt-c_6 adsorbed on C_{10}-COOH measured at various potentials. The spectral components of the reduced and oxidized protein are represented with dotted and dashed lines, respectively.

The adsorbed protein sensitively responds to the electrode potential, as evidenced by the potential-dependent spectral changes. For C_{11}-CH_3/C_{11}-OH and C_{16}-CH_3/C_{16}-OH mixed SAMs, SERR spectra can be simulated by summation of the RR component spectra of ferrous and ferric Cyt-c_6 in different proportions (Fig. 5), confirming the structural integrity of the adsorbed protein in the entire potential range explored.

In the case of C_{15}-COOH SAMs, in order to obtain a perfect reproduction of the SERR spectra at the various potentials, it is necessary to incorporate two potential-independent weak Gaussian bands at *ca.* 1349 and 1372 cm^{-1}, in addition to the Lorentzian component spectra of ferrous and ferric native Cyt-c_6 determined from the RR spectra in solution. The origin of the Gaussian bands is unclear, but the shape and potential-independence suggest that it represents a fraction of the electrostatically adsorbed protein that is redox inactive. Similar results were obtained both for WT- and M58H-Cyt-c_6.

From the component spectra, and by using the proportionality factors determined from the RR spectra in solution (*vide supra*), one can determine the relative surface concentrations of reduced and oxidized Cyt-c_6, and subsequently the standard reduction potentials through the Nernst equation (eqn (1)):

$$E = E^0 - \frac{RT}{nF}\ln\frac{[\mathrm{Cyt}^{2+}]}{[\mathrm{Cyt}^{3+}]} = E^0 - \frac{RT}{nF}\ln\frac{(I \times F)_{\mathrm{Cyt}^{2+}}}{(I \times F)_{\mathrm{Cyt}^{3+}}} \quad (1)$$

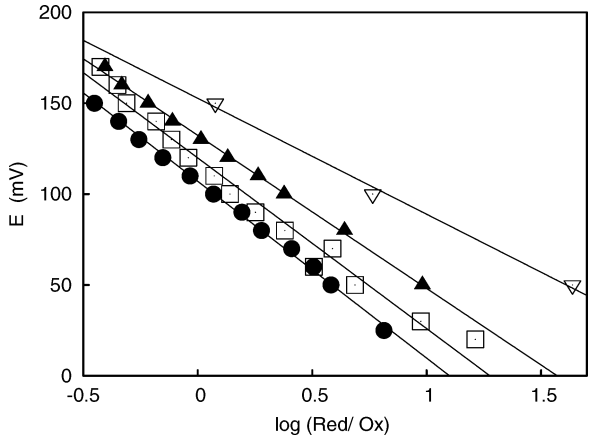

Fig. 6 Nernst plots of WT-Cyt-c_6 adsorbed on different SAMs. Circles: C_{10}-COOH. Squares: C_{15}-COOH. Up-triangles: C_{11}-CH_3/C_{11}-OH. Down-triangles: C_{16}-CH_3/C_{16}-OH.

Table 1 Standard reduction potentials (E^0) and number of transferred electrons (n) obtained for WT- and M58H-Cyt-c_6 under the different immobilization conditions

SAM	WT-Cyt-c_6 E^0/mV (n)	M58H-Cyt-c_6 E^0/mV (n)
C_{10}-COOH	114 (0.7)	−185 (0.7)
C_{15}-COOH	108 (0.7)	−199 (0.8)
C_{11}-CH_3/C_{11}-OH	150 (0.9)	n.d.
C_{16}-CH_3/C_{16}-OH	133 (0.8)	n.d.
Solution	[a]140	−140

[a] Taken from Molina-Heredia *et al.*[3]

where I and F represent the relative intensities of the spectral components and their proportionality factors, respectively. The symbols R and T have their usual meaning, and n is the number of transferred electrons. Fig. 6 shows representative Nernst plots, and the results are summarized in Table 1.

Within experimental error, the E^0 values determined for WT-Cyt-c_6 adsorbed on mixed SAMs are similar to the one reported for the protein in solution,[3] and the calculated n factors are close to the ideal value of 1.

In the case of electrostatic adsorption, the determined E^0 values, both for WT and M58H Cyt-c_6, are negatively shifted with respect to the values in solution. The shift is most likely due to the interfacial potential drop, which is expected to be more severe at charged SAMs.[27,31] Also, the n values are slightly lower compared to the uncharged SAMs, reflecting a larger heterogeneity of the electrostatically adsorbed protein. Note that, in contrast to conventional electrochemical methods, SERR probes all the adsorbed species including those that are electrochemically inactive.

Electron-transfer dynamics

The dynamics of the heterogeneous ET reactions of WT and M58H Cyt-c_6 immobilized on different SAM-coated electrodes was investigated by TR-SERR. In these experiments, the redox equilibrium of the adsorbed protein is perturbed by applying a potential jump from an initial potential E_i to a final potential E_f. SERR spectra are measured at variable delay

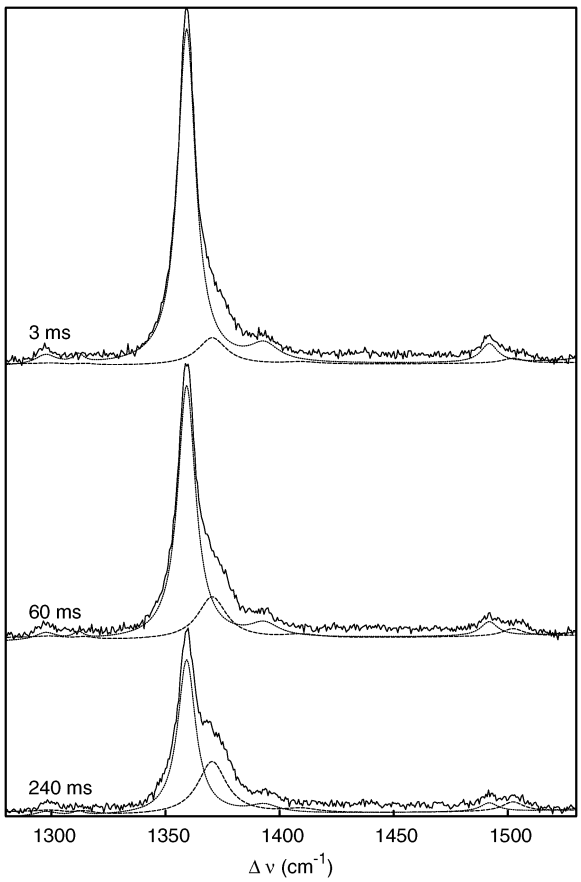

Fig. 7 TR-SERR spectra of WT-Cyt-c_6 adsorbed on a C_{16}-CH_3/C_{16}-OH SAM, measured at different delay times.

times with respect to the potential jump and analyzed in terms of ferric and ferrous Cyt-c_6 spectral components as described above. Typical TR-SERR spectra are shown in Fig. 7.

In a first approach, one may assume that the perturbed system will evolve toward the equilibrium value at the final potential following first-order kinetics with an apparent ET rate constant k_{ET}^{app}. Thus, the one-step relaxation process can be described according to eqn (2):

$$\ln\frac{[Cyt^{2+}]_{E_f} - [Cyt^{2+}]_t}{[Cyt^{2+}]_{E_f} - [Cyt^{2+}]_{E_i}} = \ln\frac{\Delta C_t}{\Delta C_0} = -k_{ET}^{app} t \qquad (2)$$

where subscripts E_f and E_i denote the equilibrium concentrations of the reduced protein at the final and initial potentials, respectively, and t is the probing delay time with respect to the applied potential jump. As shown in Fig. 8 for some representative cases, plots of the experimental data according to eqn (2) are linear within the experimental error, thus justifying the one-step relaxation assumption. The k_{ET}^{app} values obtained in this way for different experimental conditions, including different overpotentials (η), are summarized in Table 2.

First, we analyze the distance dependence of k_{ET}^{app} measured at zero driving force, *i.e.* for $E_f = E^0$ (η = 0 mV). As shown in Fig. 9, the variation of $k_{ET}^{app}(0)$ for Cyt-c_6 with the length of the SAM is qualitatively similar to the dependencies observed for mammalian cytochrome c electrostatically adsorbed on

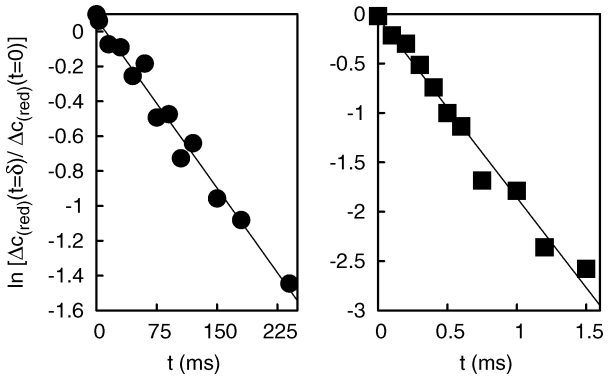

Fig. 8 Reduction kinetics of Cyt-c_6 under various experimental conditions. Circles: WT-Cyt-c_6 on a C_{16}-CH_3/C_{16}-OH SAM; η = 0 mV. Squares: M58H-Cyt-c_6 on a C_{10}-COOH SAM; η = −275 mV.

carboxyl-terminated SAMs and for other proteins immobilized on different SAM-coated electrodes.[28,32–38]

At long distances, $k_{ET}^{app}(0)$ increases exponentially upon shortening the length of the SAM, as expected for a non-adiabatic ET mechanism,[28,32–38] with a decay factor $\beta \approx 1.1$ per methylene group.

For thinner SAMs, however, the reaction rate becomes insensitive to the distance, reaching a plateau. The values determined for Cyt-c_6 display a very similar distance dependence for both charged and uncharged SAMs and are similar at each SAM thickness for zero driving force. However, the rate constants are significantly larger than for mammalian cytochrome *c* electrostatically adsorbed. The first observation is quite surprising taking into account that the protein is likely to adsorb *via* different residues to the different surfaces, and that relatively small changes of orientation are expected to result in significant variations of the electronic coupling.[30] On the other hand, the fact that ET rates for Cyt-c_6 are much larger than for mammalian cytochrome *c* is most likely the result of a stronger electronic coupling rather than a smaller reorganization energy, as both proteins share identical redox centers and quite similar heme pockets.

For the thinner SAMs studied (C_{10}-COOH and C_{11}-CH_3/C_{11}-OH), $k_{ET}^{app}(0)$ drops by *ca.* a factor of 2 upon a 50% increase of the solution viscosity (ρ). In contrast, no viscosity effect is observed for C_{15}-COOH and C_{16}-CH_3/C_{16}-OH, both for WT and M58H Cyt-c_6 (Table 2). Consistently, $k_{ET}^{app}(\eta)$ shows a clear increase with the applied overpotential (η) for

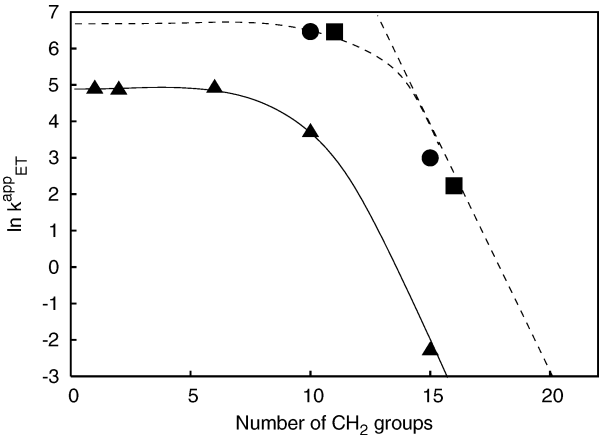

Fig. 9 Semi-logarithmic plots of apparent ET rate constants as a function of the number of methylene groups of the spacers. Triangles: horse heart cytochrome *c* on C_x-COOH SAMs. Squares: WT-Cyt-c_6 on C_x-CH_3/C_x-OH SAMs. Circles: WT-Cyt-c_6 on C_x-COOH SAMs. All values were obtained at room temperature with η = 0 mV and ρ = 1 cP.

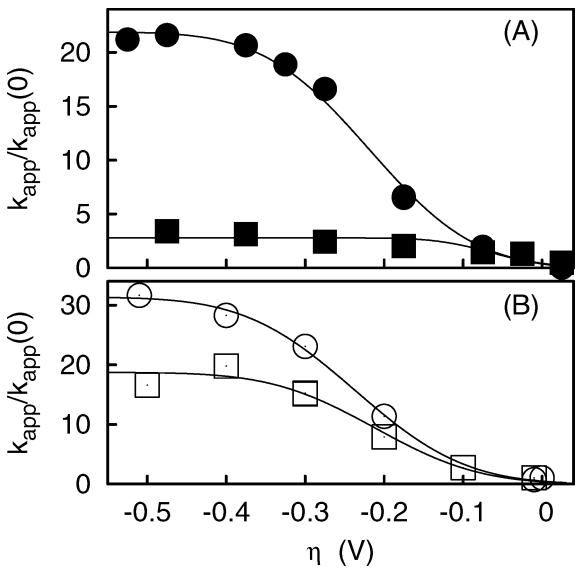

Fig. 10 Normalized apparent ET rate constants as a function of the applied overpotential. (A) M58H-Cyt-c_6 on C_{15}-COOH (filled circles) and on C_{10}-COOH (filled squares) SAMs at 1 cP. (B) WT-Cyt-c_6 on a C_{15}-COOH SAM at 1 cP (empty circles) and 1.5 cP (empty squares).

Table 2 Apparent ET rate constants obtained for WT- and M58H-Cyt-c_6 under various experimental conditions

		k_{ET}^{app}/s^{-1}		k_{ET}^{app}/s^{-1}	
		WT-Cyt-c_6		M58H-Cyt-c_6	
SAM	η/mV	ρ = 1 cP	ρ = 1.5 cP	ρ = 1 cP	ρ = 1.5 cP
C_{15}-COOH	0	20	19	66	58
C_{15}-COOH	−500	639	359	1475	259
C_{10}-COOH	0	639	302	854	419
C_{10}-COOH	−500	1230	683	2568	1040
C_{16}-CH_3/C_{16}-OH	0	9.3	8.8	n.d.	n.d.
C_{11}-CH_3/C_{11}-OH	0	637	266	n.d.	n.d.

the thicker SAMs, but nearly no change for the thinner ones (Fig. 10A).

These results suggest that at longer distances, the rate of the redox reaction is controlled by tunneling probability, while at shorter ones, a viscosity-dependent process becomes rate limiting. Note, however, that this conclusion appears to be valid only at very low driving forces. For overpotentials higher than 100 mV, an increasing viscosity effect is also observed for the thicker SAMs, reaching a $k_{ET}^{app}(\eta)/k_{ET}^{app}(0)$ ratio of *ca.* 1.7 in the plateau region (Fig. 10B).

Kinetic modeling

The results described in the preceding sections are consistent with a reaction scheme in which the measured reaction rate is a convolution of protein dynamics and tunneling probabilities, as recently demonstrated for mammalian cytochrome c.[20,30] Within this context, the simplest possible reaction mechanism that can be proposed is a two-state model,[33,39] (Scheme 1) which is also consistent with kinetic studies of Cyt-c_6/PSI interprotein complexes.[5,6,8]

In this model, it is assumed that ferric Cyt-c_6 adsorbs on the electrode surface in a thermodynamically stable orientation (O1), which does not establish an efficient electron pathway and, thus, can be regarded as redox inactive. O1 reorients to the redox-active form O2 with a rate constant k_1 and, in this configuration, accepts an electron from the electrode with a rate constant k_f. The product R1 can then reorient back to the redox-inactive form of the ferrous protein R2 (k_3). Species O1 and O2 on one hand, and R1 and R2 on the other are spectroscopically undistinguishable as they only differ in orientation.[20]

The consistency of this simplified kinetic model with the experimental results was tested numerically using a number of approximations. First, it is assumed that the surface binding energies of the four species are equal. This assumption implies that redox-linked structural changes are not significant, and that the short-range forces involved in protein binding do not depend on the oxidation state of the heme iron.

These assumptions imply $k_1 = k_4$ and $k_2 = k_3$. Second, the rate of rearrangement is considered to be independent of the SAM thickness and of the applied overpotential and is assumed to be influenced only by the medium viscosity.

The rate of diabatic heterogeneous electron transfer at a metal electrode can be expressed in terms of the high temperature limit of the Marcus semiclassical equation by integrating over all the electronic levels of the metal contributing to the process.[40] The expression can be simplified by approximating the Fermi distribution law as a step function[41] and relating the rate constants for the forward and backward ET reactions through the Nernst equation:

$$k_f(0) = A\exp(-d\beta) \quad (3)$$

$$k_f(\eta) = k_f(0)\frac{1-\mathrm{erf}[(F\eta+\lambda)/(2\sqrt{\lambda RT})]}{1-\mathrm{erf}[\lambda/(2\sqrt{\lambda RT})]} \quad (4)$$

$$k_b(\eta) = k_f(\eta)/10^{-\eta/59\ \mathrm{mV}} \quad (5)$$

where β is the tunneling decay constant, d is the distance, A is a pre-exponential factor, λ is the reorganization energy, and the other symbols have their usual meaning.

For each viscosity value (1 and 1.5 cP), entire data sets that include various driving forces and SAM lengths were simulated using A, β, λ, k_1, and k_2 as adjustable parameters. As shown in the ESI†, good fits to all experimental data recorded under various conditions are obtained for values of A, β, and λ of 1.85×10^{-12} s^{-1}, 1.07 per methylene group, and 0.35 eV, respectively. The three values are quite reasonable and are in excellent agreement with previous reports on similar redox proteins,[14,28,33–38] thus confirming that the adopted kinetic model and its underlying assumptions are justified. For a viscosity of 1 cP, the best simulations are obtained with $k_1 = 840$ s^{-1} and $k_2 = 0.5$ s^{-1}. Both values decrease at 1.5 cP to 540 and 0.2 s^{-1}, respectively. Some representative simulations are shown in the ESI†.

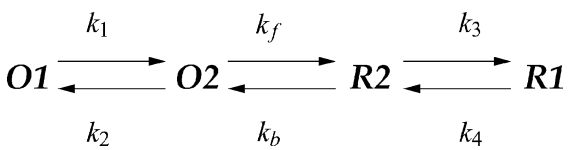

Scheme 1 Minimal kinetic model for the heterogeneous ET reaction of Cyt-c_6 adsorbed on SAM-coated electrodes. O and R denote oxidized and reduced protein, respectively. The numbers 1 and 2 refer to the redox-inactive and redox-active orientations, respectively.

Conclusions

The present results show that Cyt-c_6 can efficiently adsorb both on neutral and on negatively charged surfaces that are designed for mimicking the essential features of the interactions with its natural reaction partner PSI. SERR experiments demonstrate that the adsorbed protein retains the native structure in two types of complexes. However, in contrast to previous predictions,[4,7,8,25] the highest affinity does not correspond to electrostatic complexes but to a balance of short-range hydrophobic–hydrophilic interactions.

TR-SERR experiments performed under various conditions, including variable SAM thicknesses, viscosities, and driving forces, demonstrate that the interfacial ET reaction follows a gated mechanism. The gating step implies a rearrangement from an electrochemically inactive configuration to another one that is optimized for ET, and is consistent with previous results for Cyt-c_6–PSI complexes.[4,7,8,25] For long distances, the electron-tunneling probability is sufficiently low such that rearrangement of the complex is not rate limiting. The situation changes upon decreasing the thickness of the SAM spacer due the exponential increase of the ET rate and the relatively weak distance dependence of the rearrangement rate that, thus, becomes the rate-limiting step. Kinetic modeling of the entire data set under the different experimental conditions yields a consistent mechanistic picture with $\lambda = 0.35$ eV.

Acknowledgements

This work was supported by ANPCyT (PICT2006-459; PICT2007-00314), DFG (Sfb498-A8; Cluster of Excellence "Unifying concepts in catalysis"), the Volkswagen-Stiftung (I80816) the Spanish Ministry of Education and Science (BFU2006-01361) and the Andalusian Government (PAIDI, CVI-0198). DHM is member of CIC-CONICET. The Robert A. Welch Foundation (Grant No. E-1320) supported the work at the University of Houston.

References

1 M. Hervas, J. A. Navarro and M. A. De la Rosa, *Acc. Chem. Res.*, 2003, **36**, 798.
2 K. K. Ho and D. W. Krogmann, *Biochim. Biophys. Acta*, 1984, **766**, 310.
3 F. P. Molina-Heredia, M. Hervas, J. A. Navarro and M. A. De la Rosa, *Biochem. Biophys. Res. Commun.*, 1998, **243**, 302.
4 M. A. De la Rosa, J. A. Navarro, A. Diaz-Quintana, B. De la Cerda, F. P. Molina-Heredia, A. Balme, P. D. Murdoch, I. Diaz-Moreno, R. V. Duran and M. Hervas, *Bioelectrochemistry*, 2002, **55**, 41.
5 M. Hervas, J. A. Navarro, A. Diaz, H. Bottin and M. A. DelaRosa, *Biochemistry*, 1995, **34**, 11321.
6 M. Hervas, J. A. Navarro, A. Diaz and M. A. DelaRosa, *Biochemistry*, 1996, **35**, 2693.
7 F. P. Molina-Heredia, M. Hervas, J. A. Navarro and M. A. De la Rosa, *J. Biol. Chem.*, 2001, **276**, 601.
8 F. P. Molina-Heredia, A. Diaz-Quintana, M. Hervas, J. A. Navarro and M. A. De la Rosa, *J. Biol. Chem.*, 1999, **274**, 33565.
9 I. Diaz-Moreno, A. Diaz-Quintana, M. Ubbink and M. A. De la Rosa, *FEBS Lett.*, 2005, **579**, 2891.
10 I. Diaz-Moreno, A. Diaz-Quintana, F. P. Molina-Heredia, P. M. Nieto, O. Hansson, M. A. De la Rosa and B. G. Karlsson, *J. Biol. Chem.*, 2005, **280**, 7925.
11 I. Garcia-Rubio, M. Medina, R. Cammack, P. J. Alonso and J. I. Martinez, *Biophys. J.*, 2006, **91**, 2250.
12 I. Garcia-Rubio, P. J. Alonso, M. Medina and J. I. Martinez, *Biophys. J.*, 2009, **96**, 141.
13 D. H. Murgida and P. Hildebrandt, *Acc. Chem. Res.*, 2004, **37**, 854.
14 D. H. Murgida and P. Hildebrandt, *Chem. Soc. Rev.*, 2008, **37**, 937.
15 S. Bernad, T. Soulimane, Z. Mehkalif and S. Lecomte, *Biopolymers*, 2006, **81**, 407.
16 S. Bernad, N. Leygue, H. Korri-Youssoufi and S. Lecomte, *Eur. Biophys. J.*, 2007, **36**, 1039.
17 J. M. Ortega, M. Hervas and M. Losada, *Eur. J. Biochem.*, 1988, **171**, 449.
18 J. Grochol, R. Dronov, F. Lisdat, P. Hildebrandt and D. H. Murgida, *Langmuir*, 2007, **23**, 11289.
19 J. R. Ferraro, K. Nakamoto and C. W. Brown, *Introductory Raman Spectroscopy*, Academic Press, San Diego, 2nd edn, 2003.
20 A. Kranich, H. K. Ly, P. Hildebrandt and D. H. Murgida, *J. Am. Chem. Soc.*, 2008, **130**, 9844.
21 S. Z. Hu, I. K. Morris, J. P. Singh, K. M. Smith and T. G. Spiro, *J. Am. Chem. Soc.*, 1993, **115**, 12446.
22 P. Hildebrandt, *Cytochrome c. A multidisciplinary approach*, ed. R. A. Scott and A. G. Mauk, University Science Books, Sausalito, California, ch. 61996.
23 T. M. Bandeiras, P. N. Refojo, S. Todorovic, D. H. Murgida, P. Hildebrandt, C. Bauer, M. M. Pereira, A. Kletzin and M. Teixeira, *Biochim. Biophys. Acta*, 2009, **1787**, 37.
24 E. Droghetti, S. Oellerich, P. Hildebrandt and G. Smulevich, *Biophys. J.*, 2006, **91**, 3022.
25 A. Diaz-Quintana, J. A. Navarro, M. Hervas, F. P. Molina-Heredia, B. De la Cerda and M. A. De la Rosa, *Photosynth. Res.*, 2003, **75**, 97.
26 S. V. Atre, B. Liedberg and D. L. Allara, *Langmuir*, 1995, **11**, 3882.
27 D. H. Murgida and P. Hildebrandt, *J. Phys. Chem. B*, 2001, **105**, 1578.
28 D. H. Murgida and P. Hildebrandt, *J. Am. Chem. Soc.*, 2001, **123**, 4062.
29 J. J. Feng, D. H. Murgida, U. Kuhlmann, T. Utesch, M. A. Mroginski, P. Hildebrandt and I. M. Weidinger, *J. Phys. Chem. B*, 2008, **112**, 15202.
30 D. Alvarez Paggi, D. F. Martín, A. Kranich, P. Hildebrandt, M. A. Martí and D. H. Murgida, *Electrochim. Acta*, 2009, **54**, 4963.
31 S. Todorovic, C. Jung, P. Hildebrandt and D. H. Murgida, *JBIC, J. Biol. Inorg. Chem.*, 2006, **11**, 119.
32 D. Murgida and P. Hildebrandt, *Top. Appl. Phys.*, 2006, **103**, 313.
33 A. Avila, B. W. Gregory, K. Niki and T. M. Cotton, *J. Phys. Chem. B*, 2000, **104**, 2759.
34 Q. J. Chi, J. D. Zhang, J. E. T. Andersen and J. Ulstrup, *J. Phys. Chem. B*, 2001, **105**, 4669.
35 K. Fujita, N. Nakamura, H. Ohno, B. S. Leigh, K. Niki, H. B. Gray and J. H. Richards, *J. Am. Chem. Soc.*, 2004, **126**, 13954.
36 T. D. Dolidze, S. Rondinini, A. Verto-Va, D. H. Waldeck and D. E. Khoshtariya, *Biopolymers*, 2007, **87**, 68.
37 J. J. Wei, H. Y. Liu, D. E. Khoshtariya, H. Yamamoto, A. Dick and D. H. Waldeck, *Angew. Chem., Int. Ed.*, 2002, **41**, 4700.
38 H. J. Yue, D. Khoshtariya, D. H. Waldeck, J. Grochol, P. Hildebrandt and D. H. Murgida, *J. Phys. Chem. B*, 2006, **110**, 19906.
39 D. H. Murgida and P. Hildebrandt, *Phys. Chem. Chem. Phys.*, 2005, **7**, 3773.
40 A. M. Kuznetsov and J. Ulstrup, *Electron transfer in chemistry and biology. An introduction to the theory*, John Wiley & Sons Ltd, Chichester, 1999.
41 T. M. Nahir, R. A. Clark and E. F. Bowden, *Anal. Chem.*, 1994, **66**, 2595.